# FACTORS AND PREVENTIVE MEASURES RELATIVE TO THE HIGH TEMPERATURE CORROSION OF BLADE/DISK COMPONENTS IN FCC POWER RECOVERY TURBINES

by

**Phillip Dowson**

**Manager, Materials Engineering**

**Elliott Company**

**Jeannette, Pennsylvania**

**Douglas M. Rishel**

**Materials Engineer**

**Elliott Company**

**Jeannette, Pennsylvania**

**and**

**Norman S. Bornstein**

**Senior Research Scientist**

**United Technologies Research Center**

**East Hartford, Connecticut**

*Phillip Dowson is Manager, Materials Engineering with Elliott Company and has over 25 years experience in the turbomachinery industry. He is responsible for the metallurgical and welding engineering for the various Elliott product lines within the company. He graduated from Newcastle Polytechnic in Metallurgy and did his postgraduate work (M.S.) in Welding Engineering. He is the author/co-author of a number of technical articles related to topics such as abradable seals, high temperature corrosion, and fracture mechanics. He is a member of ASM, NACE, and ASTM.*

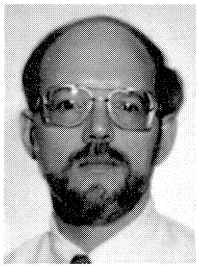

*Douglas M. Rishel is a Materials Engineer with Elliott Company. He has been involved extensively with the high temperature corrosion project. He has a B.S. degree (Mechanical Engineering) from the University of South Carolina, and M.S. and Ph.D. degrees (Metallurgical Engineering) from the University of Pittsburgh. He is a member of ASM and NACE.*

*Norman S. Bornstein is a Senior Research Scientist and Chief of Materials Processing Research at the United Technologies Research Center. He has a B.S. degree (Metallurgical Engineering) from the Polytechnic Institute of Brooklyn (1960) and an M.S. degree (Metallurgical Engineering Science) from Rensselear Polytechnic Institute (1962). He is author/coauthor of more than 30 technical articles and has been awarded 15 patents.*

## ABSTRACT

Power recovery expander turbines in the Fluid Catalytic Cracking Unit (FCCU) process operate under certain conditions that can adversely affect their performance and operational capability or integrity. For instance, erosion of the rotor blade tips by the spent catalyst can significantly reduce their efficiency and power output. Perhaps more significantly, the high temperature gaseous/catalyst environments that a power recovery turbine operates can, under certain conditions, lead to corrosive attack. This corrosive attack can cause blade failure in the location of the blade/disk root attachment where the stress intensity at the corrosive attack location exceeds the critical stress intensity necessary for fracture to occur. The fracture mechanism of Waspaloy turbine blades and how the various factors such as corrosion product morphology, depth of penetration into the alloy and a reduction in fracture toughness of the material, influence the fracture mechanism are addressed.

Since the corrosive attack is the main contributor that leads to failure, the characterization and identification of the various corrosion product phases that can form under certain gaseous/catalyst conditions will be examined. As a result of both the ability to accurately predict the susceptibility of corrosive attack and an understanding of the failure mechanism, certain protective measures can be taken. The preventive measures that have been developed by the senior author's company, such as a steam barrier system and a protective coating of the blade, are highlighted.

## BACKGROUND

In the typical refinery fluid catalytic cracking (FCC) process, crude oil stocks are converted to various petroleum products in a reactor vessel with the aid of hot catalyst. In this process, crude oil feedstocks are cracked into low boiling fractions, such as light olefins and high octane gasoline. After cracking, the spent catalyst is covered with coke deposits that must be removed prior to its reuse. In addition to carbon, heavy metals and sulfur are deposited on the catalyst surface. Recycling takes place in a regenerator, where the coke is burned off by blowing hot air. The combustion products or flue gases that result from this recycling

is a source of recoverable energy. The major components of the FCC process are illustrated in Figure 1.

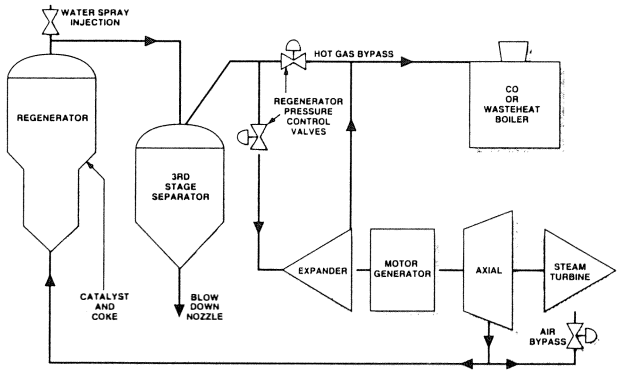


*Figure 1. Major Components Associated with the FCC Power Recovery Process.*

A power recovery turbine, or expander, is commonly used to recover energy from the discharge flue gas. Depending on customer requirements, expanders can deliver between 3,000 to 45,000 shaft horsepower. Typical flue gas inlet temperatures can range from 1200 to 1400°F at a pressure of 16 to 35 psig, whereas exhaust temperatures may range from 950 to 1100°F at a pressure of 1.0 to 3.0 psig. The mass flowrates through power recovery turbines can vary from 110,000 to 1,250,000 lbm/hr. Both single and two-stage FCC power recovery turbines are utilized in industry today. A two-stage unit is schematically illustrated in Figure 2 [1].

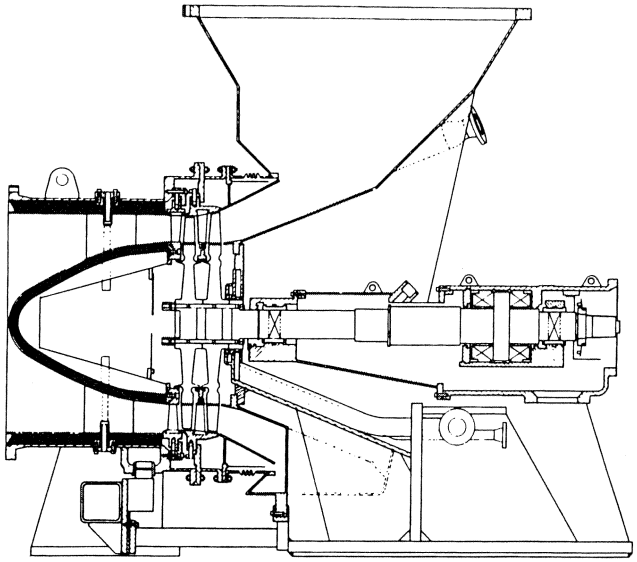

*Figure 2. Cross Sectional View of a Two-stage FCC Power Recovery Turbine.*

FCC expanders operate in environments that can be both very erosive and corrosive. The source of erosion is spent catalyst from the FCC process that has not been recovered by separators and cyclones. In general, FCC catalyst, which is very abrasive, is comprised of a mixture of zeolite, active alumina, silica-alumina, clay, rare earth oxides, and other components. Under normal operating conditions, the catalyst concentration in the flue gas is on the order of 100 ppm. During upset conditions however, the catalyst content may exceed 1500 ppm. Although erosion in FCC expanders is an important concern, the current discussion will instead focus on how both the effects of corrosion and the FCC expander environment influence the mechanical properties and subsequent life of rotating components, i.e., turbine blades. A number of factors exist that make the FCC expander environment, relative to other turbomachinery, very aggressive. These factors in part include the elevated temperatures under which expanders operate. At elevated temperatures, creep and gaseous corrosion are important concerns. Therefore, the blades and rotor disks are fabricated from either iron or nickel-base superalloys. The nature of corrosive attack is primarily influenced by the type of crude oil stock, which in turn, has a bearing on the resulting flue gas composition and the nature, and quantity of additives injected into the FCC process.

The regenerator flue gas composition can significantly change, depending on whether the regenerator is operated in a complete or partial CO combustion mode [2]. The cracking of heavy residual crude oil can result in high coke yields, which in turn, depending on the plant design, necessitates that the heat release rate be minimized. This is achieved by operating the regenerator in a partial CO combustion mode. An example of regenerator flue gas compositions is shown in Table 1. In the partial combustion mode, the combustion of CO is limited such that little or no excess oxygen exists in the flue gas, whereas in the complete combustion mode, excess oxygen with little or no CO exists in the flue gas. The FCC expander inlet temperature is also a function of the combustion process. For example, complete combustion, results in higher inlet temperatures as compared to partial combustion. For FCCs operating in the partial combustion mode, CO is typically consumed in CO boilers that are used to generate process steam. As will be discussed later, the significance of the combustion mode is related to the resulting partial pressures of gaseous oxygen and sulfur.

*Table 1. Representative Flue Gas Compositions (mol%) and Associated Equilibrium $O_2$ and $S_2$ Partial Pressure.*

| Gas Components | Partial Combustion | Complete Combustion |
|---|---|---|
| $N_2$ | 72.0 | 72.0 |
| CO | 7.4 | 0.04 |
| $CO_2$ | 11.2 | 14.4 |
| $H_2O$ | 9.3 | 11.85 |
| $O_2$ | Trace | 1.5 |
| $SO_x$ | 0.1 | 0.21 |
| Equilibrium Partial Pressure* | | |
| $P(O_2)$ | $10^{-23.5}$ | $10^{-1.9}$ |
| $P(S_2)$ | $10^{-8.8}$ | $10^{-38.0}$ |
| P(H) | $10^{-11.1}$ | $10^{-16.3}$ |
| $P(H_2)$ | $10^{-1.45}$ | $10^{-11.9}$ |
| $P(H_2S)$ | $10^{-3.0}$ | $10^{-28.1}$ |

*Calculated equilibrium partial pressures at P = 1 atm, T = 1112°F

Over the years, there has been a number of power recovery turbine blade failures that have occurred in units that operated under a partial combustion mode (for reasons unrelated to erosion, overheating, etc.). The fractures have originated in the upper land of the blade root (Figure 3). Subsequent investigations have defined the factors that may give rise to failures in this location. Several important characteristics are noted. One such feature is that relatively thick corrosion products developed in the root section of the blade and disk. These corrosion products

are primarily comprised of $Cr_2O_3$, CrS, and $Ni_3S_2$. In addition to being relatively thick, the corrosion products were found to be prone to cracking. As a result of this cracking, growth of the corrosion product into the metal substrate resulted. As described in detail later, the presence of such an oxide penetration acts as if it were a crack in the blade material. It was also observed that the fracture surfaces from the failed components were almost totally intergranular with sharp facet features. This suggests that the blade failed in a manner related to a stress corrosion mechanism. One final important feature that was observed is that the gaps between the blade root and disk were packed with spent catalyst residue. It was initially felt that this material was innocuous. However, as will be shown later, subsequent testing revealed that the catalyst residue has a detrimental effect on Waspaloy's fracture toughness.

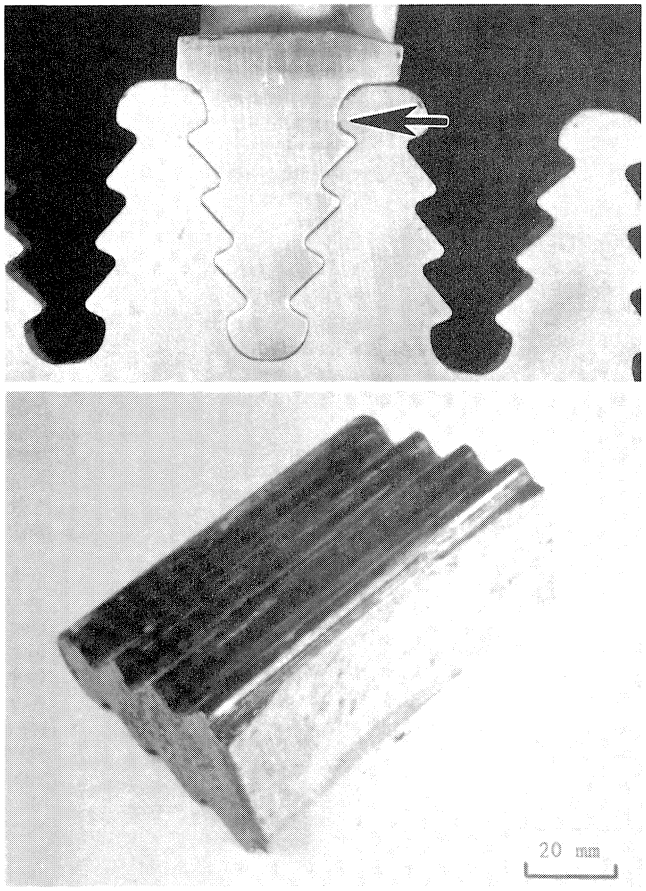


*Figure 3. Illustration of an FCC Power Recovery Turbine Blade, Showing Blade Land Location from That Fracture Originated, (As Indicated by the Arrow).*

## CORROSION PRODUCT MORPHOLOGY

The morphology of the corrosion product scale that formed on the blade roots has been found to be, in part, a function of the regenerator combustion mode and the specific location on the blade lands. Therefore, the following discussion will differentiate between the partial and complete CO combustion modes.

### *Partial CO Combustion Mode*

In a power recovery turbines, where partial combustion flue gas conditions exist, significant amounts of corrosion products were observed in the blade roots; particularly on the curved portion of the upper land. An important characteristic of the corrosion product is that it is confined to the gap that exists between the blade root and disk. Metallographic examination of the inlet and exhaust faces of the blade root, (i.e., the disk faces), revealed only a very thin oxide scale.

In the following discussion, the corrosion product morphology, which developed on a blade that had operated for approximately 39 months, is illustrated. The corrosion product, which developed on the blade root, exhibited a gold metallic-like surface appearance, Figure 4. Cross sectional examination of the blade roots and X-ray diffraction and energy dispersive X-ray analysis (EDAX) revealed this metallic-like structure to be composed primarily of $Ni_3S_2$, Figure 5. This phase is relatively brittle and friable and is easily lost during sample preparation. Subsequent cross sectional illustrations of the corrosion product scale, typically did not show the $Ni_3S_2$ phase, because it was disrupted during sample preparation.

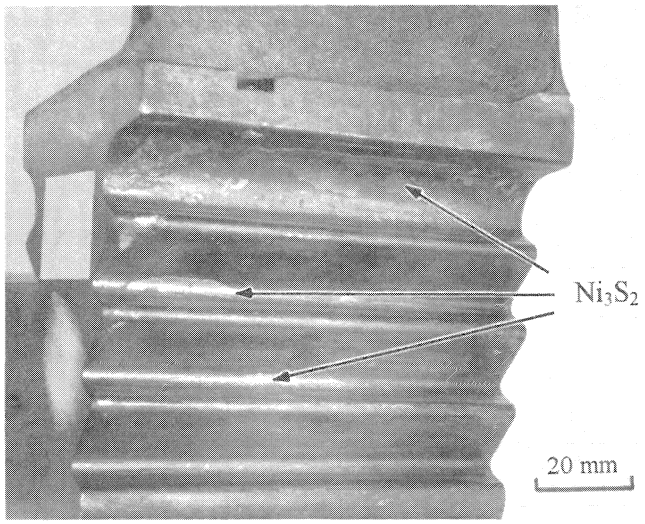


*Figure 4. Illustration of Corrosion Product Scale, Including the Presence of the "Metallic-like" Shiny Phase, on the Root Section of a Blade Removed from a Power Recovery Turbine That Operated with Partially Combusted Flue Gases.*

As alluded to earlier, variations in the corrosion product morphologies existed at different locations within the blade land. In addition, the thickness of the corrosion product, particularly that associated in the curved portion of the blade root is greater in the center of the blade root, along its axial direction. The form of the corrosion product that formed at selected locations is featured in Figures 6, 7, and 8. This series of micrographs was obtained from the axial center of the blade land.

With respect to the underlying dark gray chromium oxide structure, several features are of note and are believed to play an important role in the resulting blade fracture. First, the underlying scale, which exhibits a stratified, layered structure, can attain a substantial thickness; in some cases, on the order of 100 μm. Second, at several locations along the underlying corrosion product, cracks were observed. In the regions where cracks existed, the corrosion product significantly penetrated into the blade alloy substrate. An illustration of the corrosion product phase that existed at various locations on the curved portion of the upper root land is shown in Figure 6.

The most significant amount of corrosion product cracking appears to occur in the area adjacent to the pressure land. Due to the shape of the corrosion product penetration, this feature has been referred to as an "oxide wedge." A detailed discussion of

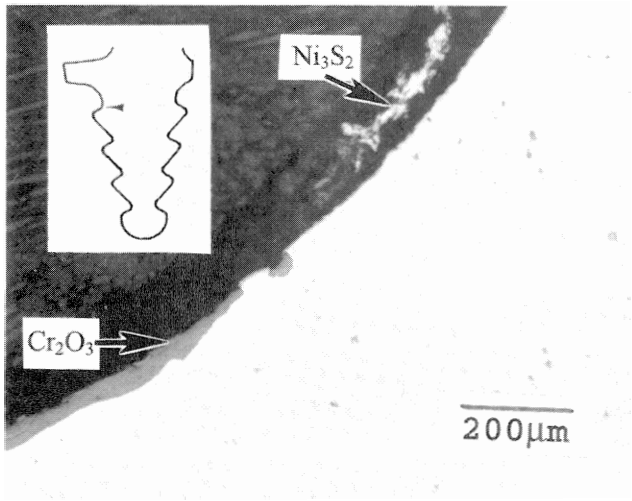


*Figure 5. Cross Sectional View of the Blade Root, in the Curved Area Adjacent to the Contact Land. Note the outer $Ni_3S_2$ phase has been disrupted and partially removed during sample preparation.*

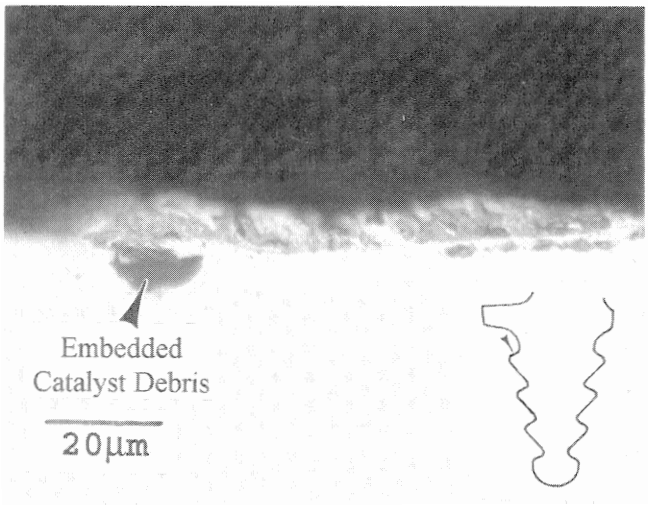


*Figure 7. Cross Sectional View of the "Kneaded" Structure That Developed on the Pressure Land of the First Root Land, for a Turbine That Operated with Partially Combusted Flue Gases. Section was taken from the axial center of the blade.*

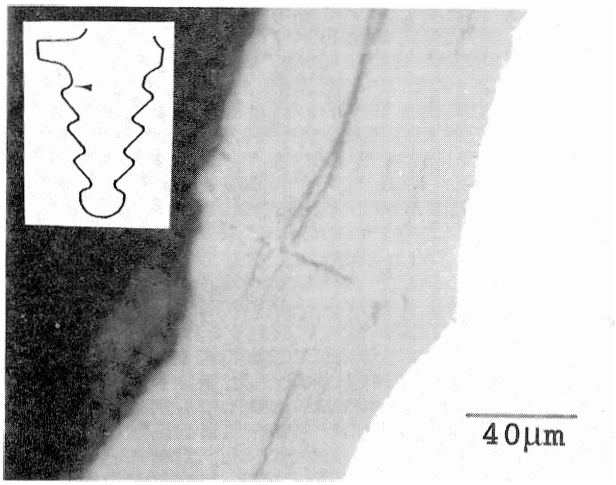


*Figure 6. Cross Sectional View of the Stratified Corrosion Product That Developed in the Curved Area of the First Root Land, for a Turbine That Operated with Partially Combusted Flue Gases. Section was taken from the axial center of the blade. (Note: The absence of the outer $Ni_3S_2$ phase is due to its disruption during blade disassembly and sample preparation.)*

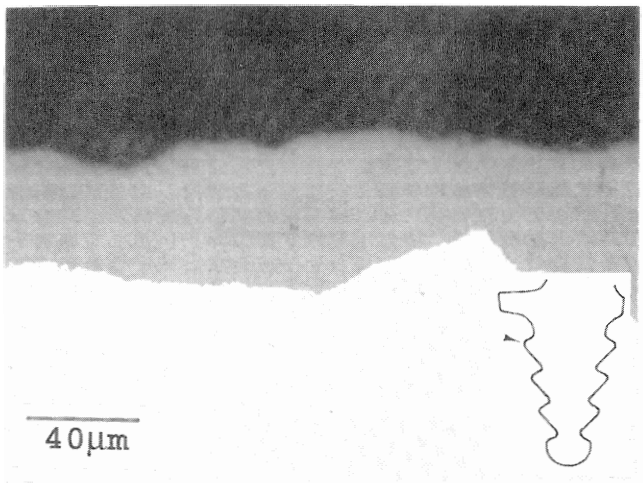


*Figure 8. Cross Sectional View of the Corrosion Product That Formed on the "Knee" of the First Root Land, for a Turbine That Operated with Partially Combusted Flue Gases. Section was taken from the axial center of the blade. (Note: The absence of the outer $Ni_3S_2$ phase is due to its disruption during blade disassembly and sample preparation.)*

oxide wedge formation and its significance will be provided later.

In the area where the blade and disk make contact, the pressure land, a complex form of corrosion product developed (Figure 7). This "kneaded" structure is comprised of a mixture of a nickel-rich metallic phase, catalyst debris, nickel sulfides and chromium oxides. The origin of such a structure is believed to be related to the relative motion between the blade and disk, i.e., fretting. Also, within the corrosion product phase and the underlying blade substrate itself, the fragments of catalyst debris are observed. The presence of catalyst fragments aids the abrasion of the pressure land contact area and the formation of the resulting kneaded structure. The corrosion product that formed along the contact land is, however, much thinner than that observed in the curved portion of the blade root.

At the corner, or "knee" of the blade land, a substantial amount of corrosion buildup has been noted, Figure 8. In this area, the corrosion buildup is primarily comprised of a chromium oxide matrix with interspersed amounts of nickel sulfide. In some observations, the resulting structure appears to have been formed by the outward extrusion of the kneaded corrosion product from the blade land.

*Complete CO Combustion Mode*

As compared to the case previously discussed, significant differences exist in the corrosive buildup that formed on the blade roots of turbines that operated on fully combusted flue gases. This difference has been consistently observed during the examination of a number units that had operated in the complete combustion mode. An example of these differences, obtained

from a unit that operated in excess of five years, on fully combusted flue gases, is shown in Figures 9, 10, 11, and 12.

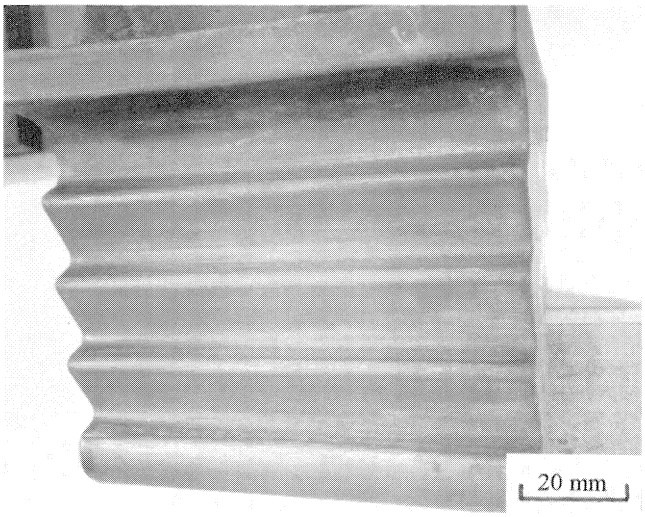


*Figure 9. Illustration of the Corrosion Product That Formed on the Root Section of a Blade Removed from a Power Recovery Turbine That Operated with Fully Combusted Flue Gases.*

Visually, the surface of the blade root (Figure 9) exhibits a dark greenish-gray color. This suggests that the corrosion product is primarily $Cr_2O_3$. In addition, as compared to blades exposed to partially combusted atmospheres (Figure 4) there is the total absence of the shiny metallic, nickel sulfide phase on the blade roots.

Within the curved portions of the blade roots, adjacent to the pressure lands, the corrosion buildup, Figure 10, is much less than that observed for blades exposed to partially combusted flue gases, Figure 6. The corrosion product observed is primarily $Cr_2O_3$ with small amounts of embedded $Ni_3S_2$. In addition, beneath the outer $Cr_2O_3$ layer and within the alloy substrate, internal precipitates of CrS were noted.

In the pressure land area, however, both blades exhibited similar features (Figures 7 and 11). In Figure 11, a mechanically

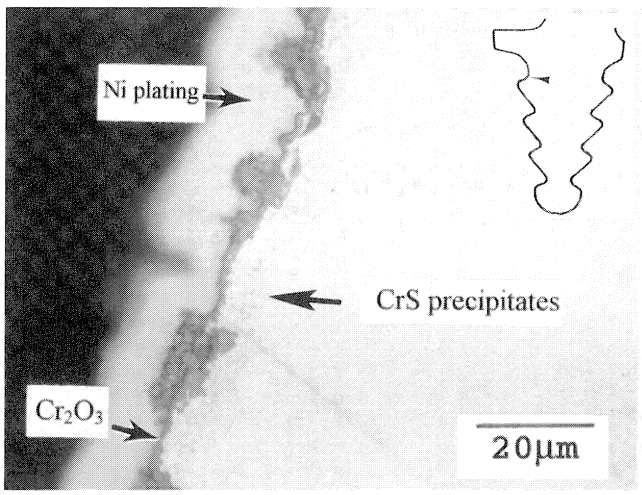


*Figure 10. Cross Sectional View of the Corrosion Product That Developed in the Curved Area of the First Root Land, for a Turbine That Operated with Fully Combusted Flue Gases. Section was taken from the axial center of the blade.*

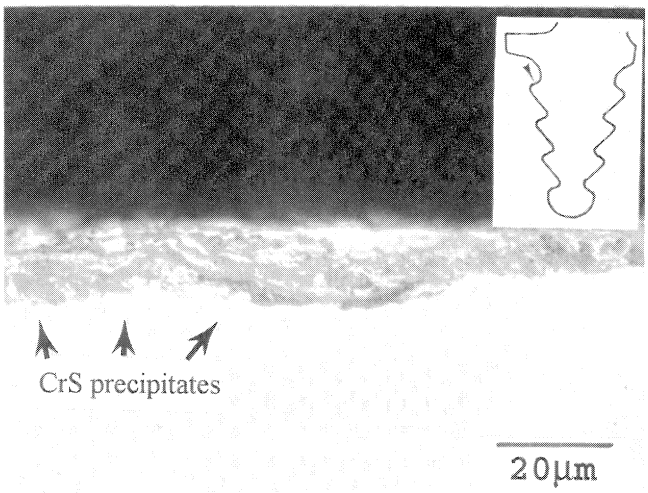


*Figure 11. Cross Sectional View of the "Kneaded" Structure That Developed on the Pressure Land of the First Root Land, for a Turbine That Operated with Fully Combusted Flue Gases. Section was taken from the axial center of the blade.*

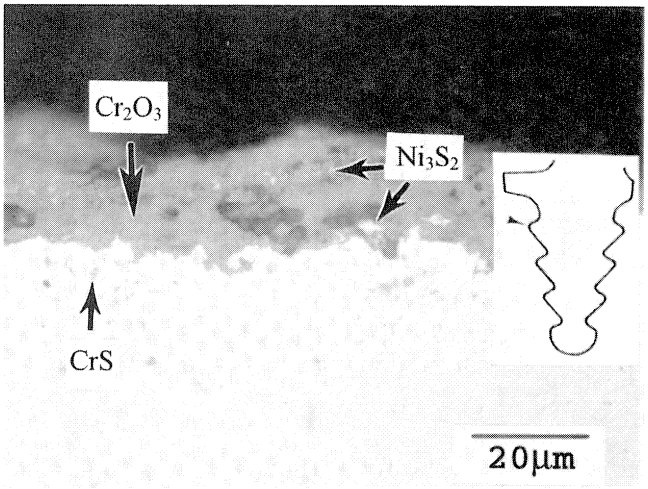


*Figure 12. Cross Sectional View of the Corrosion Product That Formed on the "Knee" of the First Root Land, for a Turbine That Operated with Fully Combusted Flue Gases. Section Was Taken from the Axial Center of the Blade.*

disrupted kneaded corrosion product, approximately 10μm thick, is illustrated. Beneath this kneaded corrosion product layer, internal precipitates of CrS are noted to exist within the alloy substrate.

In summary, there are two major differences between blades exposed to the two gaseous conditions. First, is the nature of the corrosion product that formed in the curved portion of the blade root, adjacent to, and above the pressure land. For blades exposed to partially combusted flue gases, a thick, stratified corrosion scale is developed that is comprised primarily of an outer $Ni_3S_2$ and an inner $Cr_2O_3$ layer.

The second, and perhaps most important difference between blades exposed to these conditions is the development of an oxide wedge. The formation of an oxide wedge, plays a crucial role in the fracture of expander blades. To date, oxide wedges have been observed only on blades exposed to partially combusted flue gases and appears to be related to the thickness of the

corrosion product that developed in the curved portion of the root land.

*Oxide Wedges*

The failure of blades in service have been found to occur by fracture in the upper root land with initiation on the high pressure side of the blade. The region encompassing the upper pressure land was examined from several intact blades. For units that operated on partially combusted flue gases, one feature of interest found is that related to inward oxide penetration. For the sake of this discussion, this feature is referred to as an "oxide wedge". An example of the shape and location of an oxide wedge is illustrated in Figure 13.

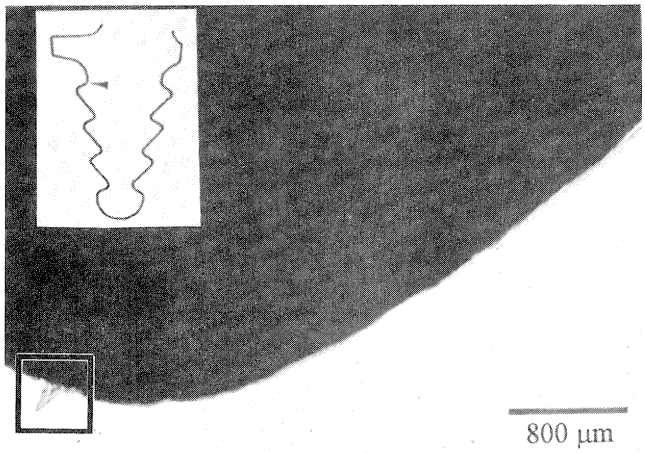


*Figure 13. Cross Sectional View of the Stratified Corrosion Product, and "Oxide Wedge" (in the Highlighted Area) That Developed in the Curved Area of the First Root Land, for a Turbine That Operated with Partially Combusted Flue Gases. Section was taken from the axial center of the blade. (Note: The absence of the outer $Ni_3S_2$ phase is due to its disruption during blade disassembly and sample preparation).*

In Figure 14, an oxide wedge is shown in greater detail, along with X-ray images for Cr, Ni, Co, S and O. It appears that the oxide wedge, is for the most part comprised of $Cr_2O_3$ with the above elements and Ti, Al and Mo existing in solid solution. The exception is the crack in the oxide wedge center, which is filled with a phase rich in Ni, Co and S. It was also interesting to observe that the crack in the oxide wedge center, propagates or grows into the Waspaloy blade substrate in a transgranular manner. This is illustrated in Figure 15, which is a high magnification micrograph of the oxide wedge tip shown in Figure 14.

Detailed metallography has been used to find that the size and depth of the oxide wedge penetration, varies along the length of the blade land. For a given load, the minimum penetration depth occurs near the inlet and exhaust faces of the blade root, whereas the maximum penetration occurs near the axial blade root center. In the case of the oxide wedge shown in Figure 14, which was taken from the center of the blade root in the axial direction, the oxide wedge penetrates approximately 280 μm into the blade substrate.

It was also observed that oxide wedges exist on either side of the blade root. However, their size and penetration depth decreased as the blade land moved radially inward, (i.e., closer to the rotor shaft). The oxide wedge is illustrated in Figure 16 associated with the third blade land, which extends to a depth of 70μm.

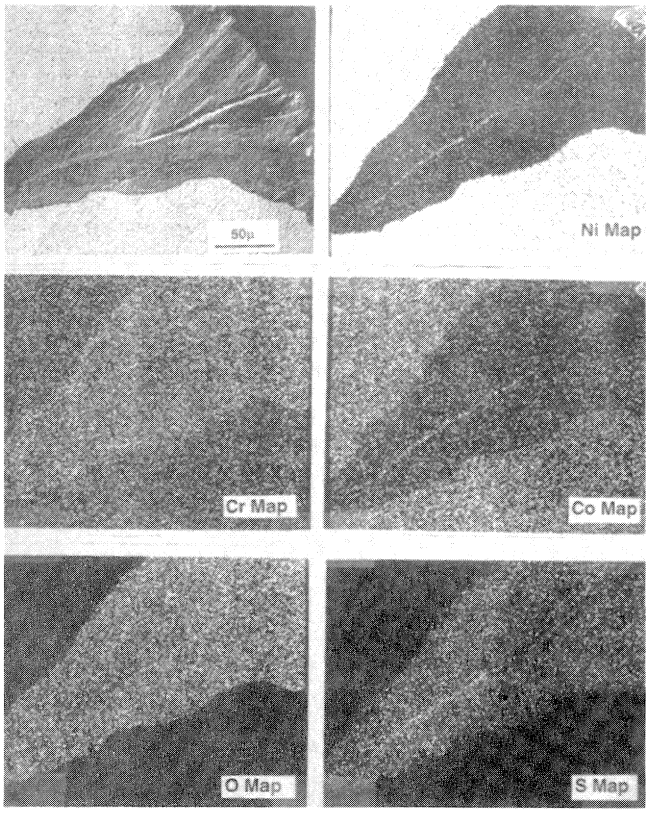


*Figure 14. Cross Sectional Sem Micrograph of the Oxide Wedge, Shown in the Highlighted Area of Figure 13 and the Corresponding X-Ray Images for Cr, Ni, Co, S, and O.*

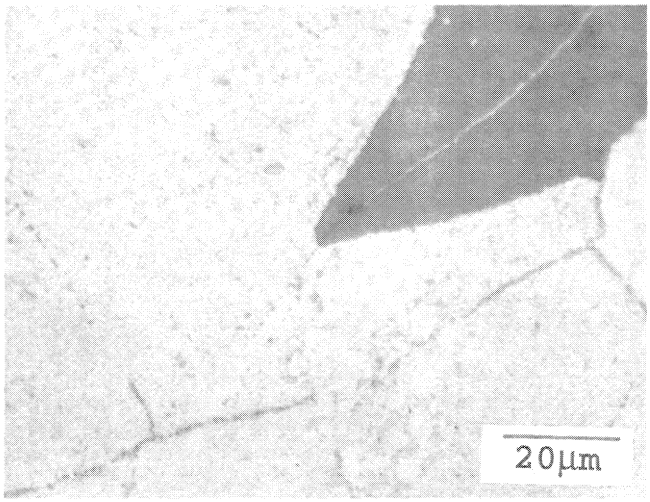


*Figure 15. High Magnification Cross Sectional View of the Tip of the Oxide Wedge Shown in Figure 14.*

To reiterate, oxide wedges are observed only on blades from turbines that have operated under partial combustion conditions and that exhibited a thick, stratified chromium oxide rich inner layer. Oxide wedges have not been observed, to date, on units that operated under complete combustion conditions. In contrast to the blades that operated under partial combustion conditions, an example is illustrated in Figure 17 of the type of corrosion product that formed on a blade that operated under complete combustion conditions. Note the lack of a stratified oxide scale

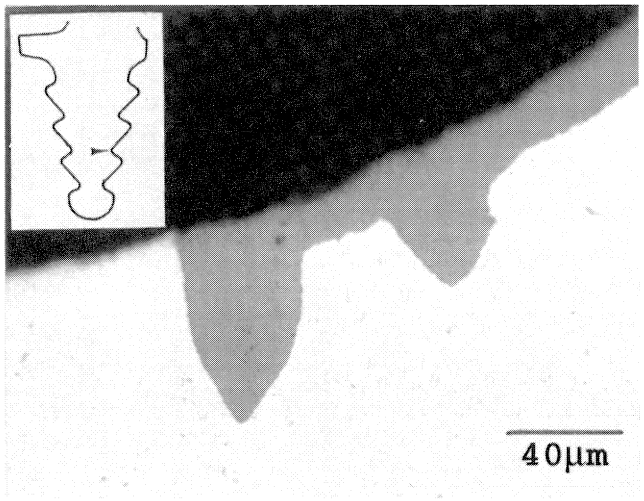


*Figure 16. Cross Sectional View of the Oxide Wedge That Formed on the Third Blade Root Land, for a Turbine That Operated with Partially Combusted Flue Gases.*

and the formation of an oxide wedge. This micrograph was taken from the same location on the blade root that exhibited oxide wedge formation under partial combustion conditions.

Oxide wedge formation is a form of oxidation damage related to the repeated crack nucleation and growth of the oxide layer at the oxide wedge tip. The rupture of the oxide layer at the wedge tip exposes the alloy substrate to the corrosive environment. The role of thermomechanical fatigue, creep and oxidation (and in particular the oxidation damage due to wedge growth) has been examined by Sehitoglu [3] for steels, Ni-based superalloys, and Al alloys. In a model developed by Sehitoglu [3] to describe oxide wedge growth, the mechanisms leading to wedge growth incorporated such factors as temperature, strain rate, strain range and strain-temperature phasing.

Two types or forms of oxide wedge growth are reported. In what is described as Type I wedge growth, oxide intrusions with a "continuous" oxide layer formed along the environmentally exposed surfaces that includes the crack faces. Type II growth is characterized as the growth of oxide "intrusion" with "stratified" oxide layers. When the stratification reaches a certain thickness, the oxide fractures and crack growth is channeled into the substrate. The Type II oxide intrusion growth, as described by Sehitoglu [3], appears to approximate the oxide wedge growth observed on the blade roots of power recovery turbines operating with partially combusted flue gases.

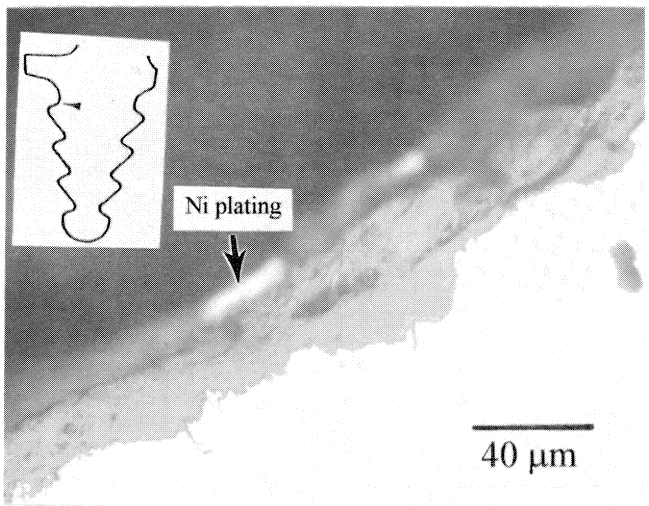


*Figure 17. Cross Sectional View of the Blade Root Land, for a Turbine That Operated with Fully Combusted Flue Gases. Micrograph was taken in the area prone to oxide wedge formation in units operating with partially combusted flue gases.*

In the model developed by Sehitoglu [3], two strain components contribute to oxide wedge growth; strains associated with mechanical loads and strains due to thermal cycling. Type II oxide growth appears to predominate when the strains associated with the mechanical load and thermal cycling are out of phase, and as the strain component due to thermal cycling approach zero, (i.e., $\Delta T = 0$). The conditions necessary, as described by Sehitoglu, for Type II oxide growth are in qualitative agreement with the conditions encountered in power recovery turbines where oxide wedge growth occurs. Power recovery turbines operate primarily under constant operating conditions, for long periods of time, where the strain components are predominantly due to mechanical loading and not thermal cycling.

*Corrosion Considerations*

The description of the corrosion of metals and alloys in gases containing two or more oxidants (e.g., $O_2$, $SO_x$, $H_2S$, CO, $CO_2$, and $N_2$) is complex. In general, the effect of the second oxidant involves its penetration through an external oxide film to form sulfides, carbides or nitrides beneath the alloy/oxide interface. The extent to which a second oxidant phase forms, is in large measure related to thermodynamics and kinetics. An understanding of the thermodynamic considerations, under partial and complete CO combustion conditions is conveniently described in terms of thermodynamic stability diagrams [4]. Such diagrams (Figure 18) are constructed for a given metal by plotting the logarithmic values of the activities or partial pressures of the two nonmetallic components (e.g., $O_2$ and $S_2$) as the coordinate axes.

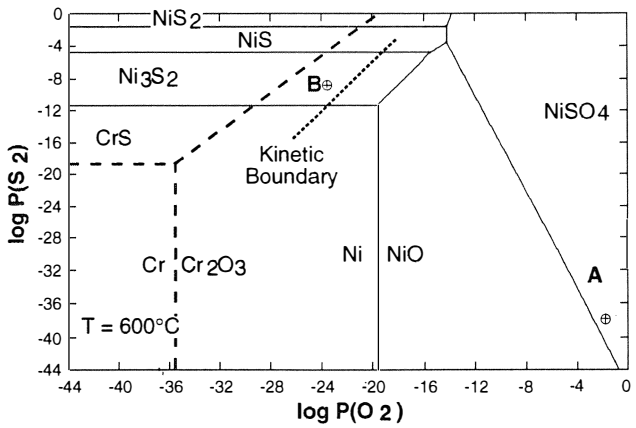


*Figure 18. Superimposed Thermodynamic Stability Diagrams for the Ni, Cr, S and O Systems at 600°C. Point A Corresponds to an "Oxidizing" Environment Typical of Fully Combusted Flue Gases. Point B corresponds to a "sulfidizing" environment typical of partially combusted flue gases.*

The thermodynamic stability diagram shown in Figure 18 was constructed by the simple superposition of diagrams for the pure metals Cr and Ni at 600°C. Also indicated in Figure 18 is the equilibrium $S_2$ and $O_2$ partial pressures for the partial and complete combustion conditions listed in Table 1; (the corrosion conditions established by the high $S_2$ and low $O_2$ partial pres-

sures is sometimes referred to as sulfidizing, whereas the conditions established by the low $S_2$ and high $O_2$ partial pressures are referred to as oxidizing). The authors' company has successfully developed a means of determining the $S_2$ and $O_2$ partial pressures, with systems containing multiple species, through the use of computer programs designed to calculate equilibrium conditions.

The following discussion will focus on the effects of mixed oxidation, or more specifically the sulfidation-oxidation behavior of Waspaloy in FCC related environments. A more in depth discussion, on the sulfidation-oxidation of various alloys of industrial importance can be found in the literature, [5, 6, 7]. In a Ni-base superalloy, such as Waspaloy, the selective oxidation of Cr to form $Cr_2O_3$ is relied upon to provide high temperature corrosion resistance. In the power recovery turbine environment, an important additional oxidant is sulfur. The major effect of sulfur, involves its penetration through the external $Cr_2O_3$ film to form sulfides beneath the alloy/oxide interface. Sulfur will react with Cr to form CrS and thus enhance the depletion of these elements from the alloy. The subsequent oxidation of these phases often results in the formation of discrete $Cr_2O_3$ particles rather than a continuous protective film. In addition, the depletion of Cr results in an increase in the activity of the base metal, Ni, which can result in the corrosion products becoming enriched in these elements. This generally results in more rapid rates of corrosion and, in certain cases, the catastrophic corrosion due to liquid sulfide formation.

The depletion of Cr also results in an increase in the activity of the base metal, Ni, and increases the driving force for the outward migration of these elements through an existing scale. This phenomenon can be of critical importance in atmospheres where the sulfur partial pressure is high. Such is the case for power recovery turbines operating on partially combusted flue gases. In this case, the oxide of Cr is stable in the gas but the sulfide of Ni is stable relative to its corresponding oxide. The occurrence of significant concentrations of Ni (and to a lesser degree Co) at the scale/gas interface can result in sulfide formation.

The equilibrium $S_2$ and $O_2$ partial pressures, which give rise to a transition from protective oxidation to rapid sulfidation, occurs over a narrow range of gas compositions. For a given alloy system, such as Waspaloy, a boundary may be constructed on the thermodynamic stability diagram, (Figure 18) [6, 7, 8]. Above, and to the left of this boundary, rapid sulfidation occurs, whereas below, and to the right of this boundary protective oxidation is observed. Such a boundary does not correspond to any of the phase boundaries on the stability diagrams for individual alloy components. Instead, this boundary will fall between the sulfide/oxide boundaries for Cr and that for Ni, [8].

The transition boundary has also been described as the kinetic boundary, (KB), [5, 6]. The kinetic boundary is defined as the $O_2$ partial pressure necessary for a continuous $Cr_2O_3$ layer to develop on an alloy surface. Typically, this is $10^2$ to $10^3$ times higher than the $Cr_2O_3$ to CrS equilibrium values. Following Xu, et al., [6] a general schematic model describing the corrosion of an alloy, on both sides of the KB, is shown in Figure 19. If the equilibrium $S_2$ and $O_2$ partial pressures lie to the left of the KB, (such as in the case if the oxygen partial pressure is sufficiently low and the sulfur partial pressure is sufficiently high), a fast growing sulfide layer is expected to rapidly overgrow the $Cr_2O_3$ scale after the initial stage of oxidation. Eventually, the alloy is covered by a thick layer of sulfides. Under such conditions, no protection is available and severe corrosive attack is expected.

For gas compositions lying to the right and below the KB, the growth of a stable $Cr_2O_3$ scale will suppress the formation of sulfides. Initially, a continuous $Cr_2O_3$ layer is built up. During

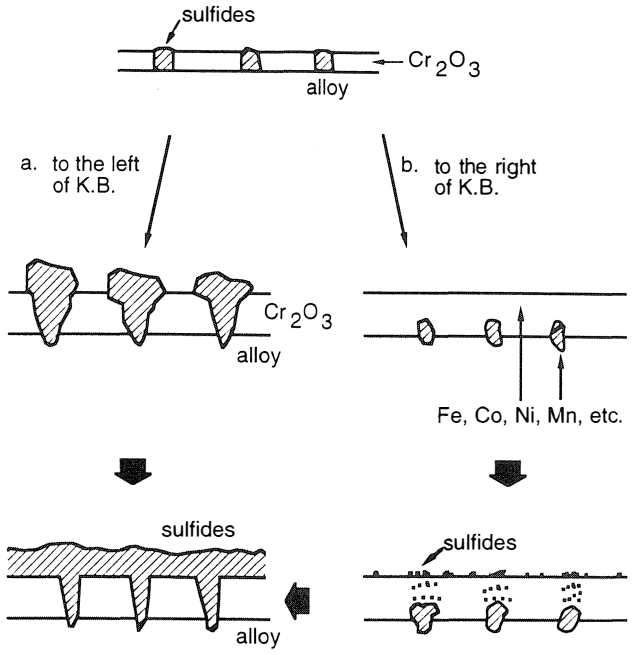


*Figure 19. Following Xu, et al. [6], a Schematic Representation of the Anticipated Corrosion Product Morphology on Each Side of the Kinetic Boundary (KB).*

this time, the protectivity of the oxide scale is maintained. The outward diffusion however, of Ni through the $Cr_2O_3$ layer cannot be stopped and eventually $Ni_3S_2$ ducts form. In addition, $Ni_3S_2$ granules will form on the $Cr_2O_3$ scale above the sulfide ducts, [9]. Given sufficient time, sulfide channels will be set up across the oxide, and rapid or breakaway corrosion occurs.

Two distinctly different corrosion product morphologies have been observed within the blade root/disk gap and on the exposed root faces. A summary illustration of the corrosion products described above is shown in Figure 20. (Note: In this figure, the

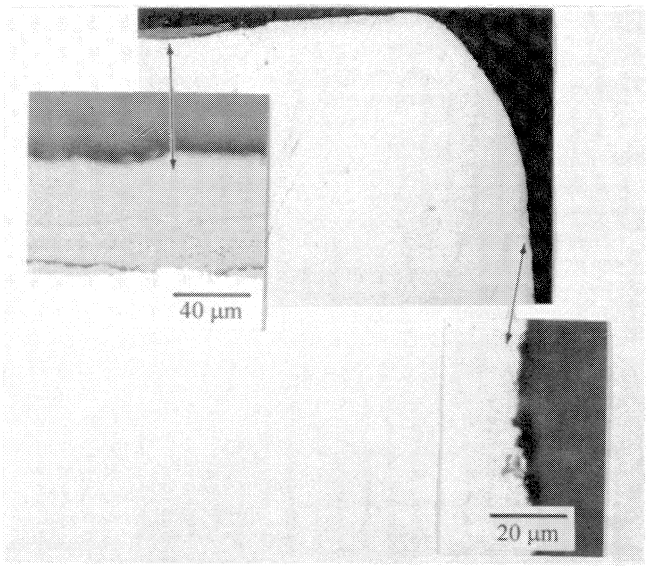


*Figure 20. Observed Corrosion Product Morphologies Within the Blade Root/disk Gap and on the Exposed Surface of the Blade Root. Blade was taken from a unit that operated on partially combusted flue gases.*

outer $Ni_3S_2$ layer found within the blade root/disk gap was disrupted during blade removal and sample preparation). The fact that two different corrosion product morphologies were observed suggests that the local environments within the blade root/disk gap and at the exposed root faces are distinctly different. Two possibilities exist that may account for the change in the "local" environment within the blade root/disk gap. The first possibility is related to the fretting wear observed on the pressure land.

As a result of fretting, the nominally protective $Cr_2O_3$ film is disrupted, and slivers of "fresh" Waspaloy is exposed to the environment. Upon further exposure, the more reactive elements, Cr, Al and Ti are preferentially oxidized. This action enriches the slivered material with the less reactive elements of Ni and Co. This interpretation is based upon electron microbeam probe analysis of the kneaded structure, where the active elements, (principally Cr, Al and Ti) were not present, or are present as finely divided oxide particles. The metallic portion of the kneaded structure was found to consist principally of Ni. It was postulated that the kneaded material can perform as a potential sulfur reservoir by first reacting with the environment to capture sulfur and by later aiding in the transfer of sulfur into the Waspaloy substrate.

This hypothesis was tested in experiments whereby pure nickel was bonded to Waspaloy coupons, via hot isostatic pressing, and exposed to sulfur bearing atmospheres at elevated temperatures. An example of the results of such a test is shown in Figure 21, for a coupon exposed for eight hours at 1340°F in an atmosphere consisting of $H_2$, $H_2S$, $CO_2$ and CO with equilibrium partial pressures of $P(O_2) = 10^{-21.8}$ and $P(S_2) = 10^{-8.1}$. In the region where the Ni was bonded to Waspaloy, a significant corrosion reaction occurred. The reaction products were determined to be primarily CrS and $Ni_3S_2$.

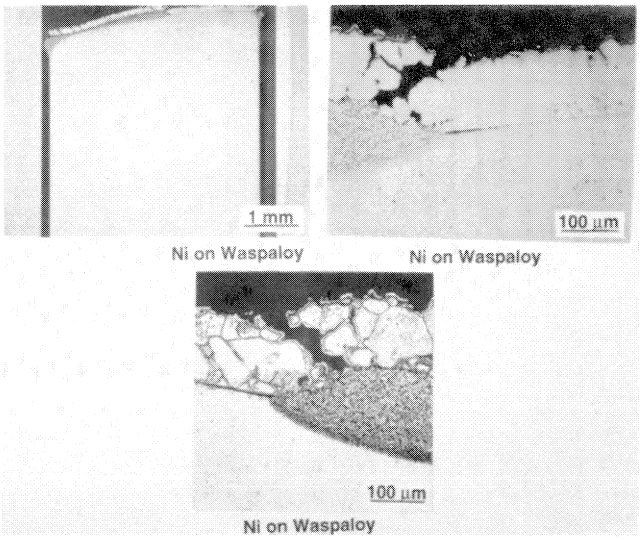


*Figure 21. Cross Sectional View of the Corrosion Reaction That Occurred on a Coupon Where Pure Nickel Was Bonded to a Waspaloy Coupon. The coupon was exposed to an environment consisting of $H_2$, $H_2S$, CO, and $CO_2$ at 1341°F for eight hours. The equilibrium partial pressures were $P(O_2) = 10^{-21.8}$ and $P(S_2) = 10^{-8.1}$.*

In regions of the coupon removed from the bonded Ni, a protective $Cr_2O_3$ film developed on Waspaloy. Thus, this test illustrates that the presence of a Ni-rich phase over a Waspaloy substrate effectively "shifts" the expected corrosion behavior from the right side of the K.B. to the left.

In addition to fretting, it is possible for Ni-rich phases to exist or accumulate within the blade root/disk gap. Two possible sources include Ni-bearing lubricants that may have been used during the assembly of the rotor disk, and the accumulation of Ni, on the catalyst residue that may accumulate within the blade root/disk gap. The source of Ni in this instance is from the crude oil stocks cracked in the FCC process.

The second possible means by which the local environment may be altered is related to the accumulation of catalyst debris within the blade root/disk gap. The possibility of the catalyst altering the local environment arose as the result of a chemical analysis that was conducted on spent catalyst. This catalyst was obtained from a separator in a FCC unit that operated in a partial CO combustion mode. In addition to the elements associated with catalyst particles, trace amounts of such elemental species as V, Ca, Na, Ni, K, Mg, Ba, Sb and Pb were detected. Elements such as V, Na, and Ca are of concern due their role in deposit-modified (Hot) corrosion [4, 10]. The heavy metals Sb and Pb are of a concern due to their adverse affect on Ni-base superalloy mechanical properties. In addition to the above listed elements, significant amounts of C and S were measured, 0.34 and 0.11 wt percent, respectively.

The origin for most of the trace elements, (V, Ca, Na, Ni, K, Mg and Ba), is most likely related to the crude oil that was cracked and the steam that was injected into the power recovery turbine. The origin of the heavy metals, such as Sb on the spent catalyst, is most likely due to their intentional injection into the crude oil charge. The reasons for this addition were described by Gilson and McKay [11]. Metals such as nickel and vanadium, which naturally occur in crude oil, act as dehydrogenation catalysts when deposited on equilibrium cracking catalysts in the FCCU. The dehydrogenation reactions increase FCCU hydrogenation and coke yields, and decrease gasoline yield. In turn, the increased hydrogen and coke yield reduces the oil charge volume the FCCU can process due to increased loads on FCCU air blowers and gas compressors. Antimony is a very efficient passivant of nickel and vanadium when deposited on the equilibrium catalyst.

The effective passivation occurs by antimony both reacting with nickel to form an alloy on the catalyst and covering the metals on the catalyst surface. The result of antimony passivation of nickel and vanadium is for many FCCUs to increase the oil charge rate, charge lower quality oil, increase conversion and improve the selectivity to higher value cracked products. The use of antimony, as a metal passivant, was first used commercially in heavy oil FCCUs with about 3,800 ppm Ni and 6,900 ppm V on the equilibrium catalyst.

To assess the role played by spent catalyst, special tests were conducted, using seamless Waspaloy tubing. Samples of spent catalyst were placed into Waspaloy tubes, the tube ends crimped closed and heated to 1292°F for 120 to 168 hr. From these simple tests, two important results were derived. First, with only the catalyst present, significant amounts of corrosion a layer ≈ 40 µm thick was observed (Figure 22). Analysis with EDAX indicated the corrosion product to be comprised primarily of Cr, Ni, O and lesser amounts of S.

The second feature observed was the cracking of the Waspaloy tubing itself (Figure 23). The observed cracking was intergranular and exhibited brittle characteristics. It also appeared that the cracking was related in some manner to stress in that the cracks originated from the tube ends and propagated to the tube center. In regions near the tube center, where the stresses were expected to be small, crack growth was arrested. As a result of these observations, a set of experimental tests were undertaken

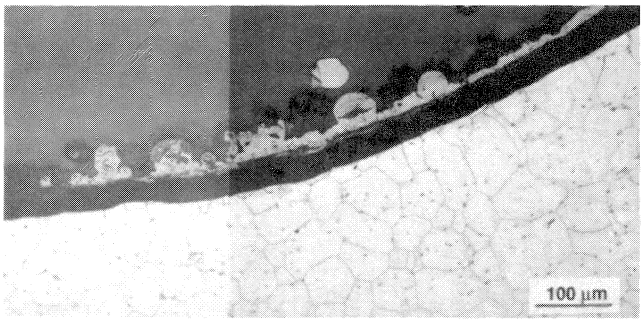


*Figure 22. Corrosion Product Formation That Occurred on the Inside Wall of Waspaloy Tubes Filled with Spent FCC Catalyst after 168 Hr. At Temperatures of 1292°F.*

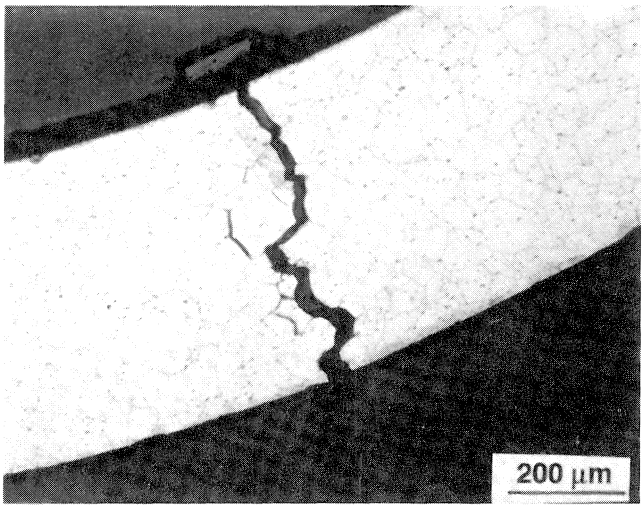


*Figure 23. Crack Formation That Occurred in a Waspaloy Tube Filled with Spent FCC Catalyst after 168 Hr at 700°C. Crack originated from the tube inner wall and propagated outward.*

in an effort to quantify a relationship between stress, temperature and the onset of cracking in catalyst environments.

## HIGH TEMPERATURE MECHANICAL TESTING

The influence of catalyst on the mechanical properties of Waspaloy is illustrated from a series of stress-rupture tests that were conducted under, what can be described as, three different sets of "environmental conditions." All tests were conducted from the same heat of AMS 5704, Waspaloy bar. The analyzed chemical composition of the Waspaloy bar used in the following tests is shown in Table 2.

For two of the condition sets, notched combination creep-rupture specimens were machined from the as received Waspaloy bar, in accordance with ASTM E292. In Set #1, the machined specimens were directly tested in air atmospheres. Prior to conducting Set #2 experiments, the machined specimens were given a sulfur impregnation treatment. This treatment was performed using an evacuated quartz tube, backfilled with Argon that contained the notched combination specimen and small amount of sulfur flour. The sealed quartz tube was then heat treated at 1472°F for 100 hr. This treatment resulted in the formation of internal CrS precipitates, internal to the Waspaloy substrate (Figure 24).

Set #3 tests involved evaluating a specially modified creep-rupture bar (Figure 25). The machined specimens were inserted into a specially designed stainless steel "jacket" (Figure 25) that

*Table 2. Analysis of Waspaloy Bar Used in the High Temperature Mechanical Testing Experiments.*

| In Weight Percent | | | |
|---|---|---|---|
| C | 0.036 | Mn | 0.046 |
| S | 0.001 | Cr | 20.11 |
| P | 0.010 | Si | 0.14 |
| Cu | 56.88 | Mo | 3.85 |
| Co | 13.15 | B | 0.005 |
| Fe | 1.13 | Zr | 0.055 |
| Ti | 3.11 | | |
| | In PPM | | |
| | PB *5 | | |

*Not Detected; Number indicates the minimum limit of detection.

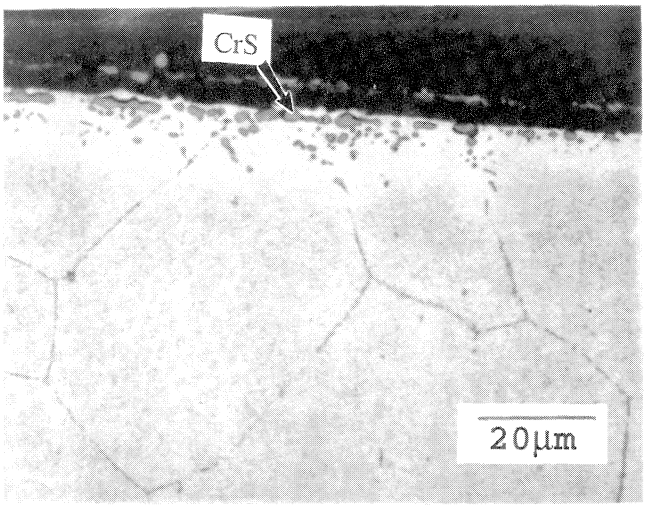


*Figure 24. Illustration of Internal CrS Precipitates That Formed in a Waspaloy Coupon Heated in a Quartz Tube, Containing Sulfur Flour at 1472°F for 100 Hr.*

was filled with 33 gms of spent FCC catalyst. A quantitative chemical analysis of the catalyst is shown in Table 3. The metallic species present were assumed to exist in the oxide form. The test conducted with the catalyst were referred to as "modified catalyst stress-rupture" tests.

The combination stress-rupture bars listed above were exposed under the load and temperature combinations listed in

*Table 3. Catalyst Used in "Modified Stress-Rupture" Tests.*

| Dry Basis (in Weight %) | | | |
|---|---|---|---|
| C | 0.34 | | |
| S | 0.11 | | |
| Other Species (in Weight %) | | | |
| $SiO_2$ | 60.00 | NiO | 0.19 |
| $Al_2O_3$ | 30.66 | CaO | 0.12 |
| $TiO_2$ | 3.95 | $K_2O$ | 0.12 |
| SrO | 2.00 | MgO | 0.086 |
| $Fe_2O_3$ | 0.99 | $Sb_2O_3$ | 0.067 |
| $V_2O_5$ | 0.83 | BaO | 0.063 |
| $Na_2O$ | 0.55 | PbO | 0.048 |

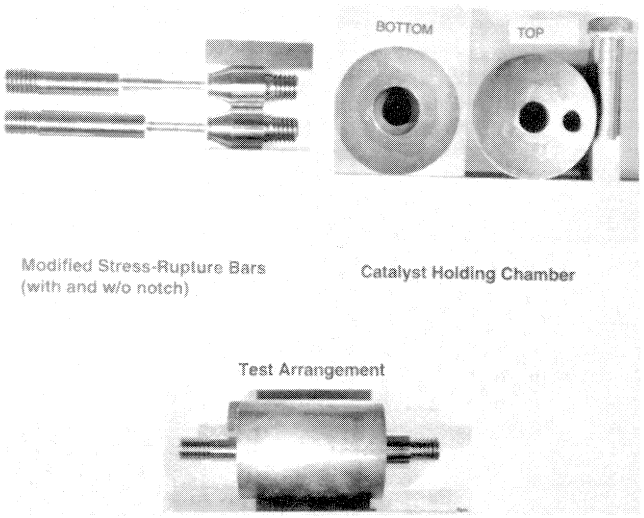


*Figure 25. Illustration of the Modified Catalyst Stress-rupture Test Arrangement with the Catalyst Holding Chamber and Modified Stress-rupture Bar.*

Table 4. Stress-rupture tests conducted on the as received and sulfur impregnated specimens found that the specimens failed due to creep. As listed in Table 4, the failure times were typically in the hundreds of hours. In addition, specimens exposed under these conditions did not exhibit notch sensitivity; all failed in the smooth section of the specimen. As compared to the specimen tested under Set #1, the S-impregnated bars of Set #2, when metallographically examined, exhibited a significant greater amount of creep cavitation.

*Table 4. Stress-Rupture Test Results.*

| *As Received Material Results* | | | |
|---|---|---|---|
| *T (°F)* | *Load (lb.)* | *$T_f$ (hr)* | *Location* |
| 1292 | 1,742 | 663.3 | Smooth Section |
| 1202 | 2,364 | 931.3 | Smooth Section |
| 1112 | 2,737 | 2667+ | Did Not Fail |
| *S-Impregnated Results* | | | |
| *T (°F)* | *Load (lb.)* | *$T_f$ (hr)* | *Location* |
| 1292 | 1,742 | 259 | Smooth Section |
| 1202 | 2,364 | 350 | Smooth Section |
| 1112 | 2,737 | 346 | Smooth Section |
| *Catalyst Filled Chamber Results* | | | |
| *T (°F)* | *Load (lb.)* | *$T_f$ (hr)* | *Location* |
| 1292 | 1,742 | 0.2 | Notch |
| " | 1,742 | 2.3 | Notch |
| " | 1,269 | 0.9 | Notch |
| " | 846 | 334.5+ | Did Not Fail |
| " | 846 | 333.6+ | Did Not Fail |
| 1202 | 2,364 | 3.3 | Notch |
| " | 1,717 | 355.6+ | Did Not Fail |
| 1112 | 2,737 | 13 | Notch |
| " | 2,737 | 12.2 | Notch |
| " | 2,165 | 32.7 | Notch |

In the case of the modified catalyst stress-rupture tests, Set #3, significant and important differences were found. Under these condition, rapid failure, on the order of minutes, occurred in the notched section of the specimen. As shown in Figure 26, failure occurred via intergranular crack propagation.

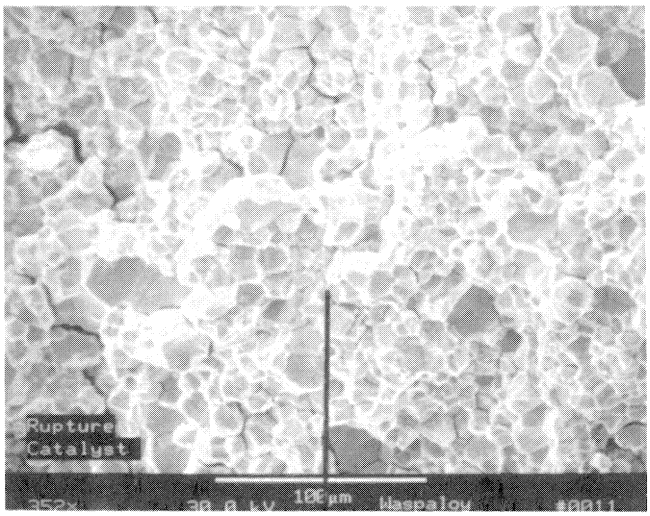


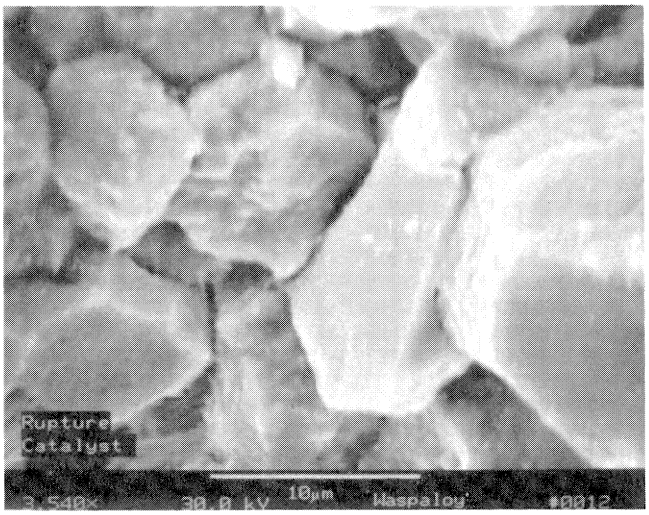


*Figure 26. Fracture Surface of a Specimen Tested under Modified Catalyst Stress-Rupture Tests. Exposure Condition: T = 1292°F, P = 1,742 lb., $T_f$ = 20 minutes.*

In an effort to ascertain what species may have been responsible for this rapid failure, special test bars were made in order to examine, a sample that had been exposed to a catalyst environment, under load and at elevated temperature, in a scanning auger electron microscope. Auger electron microscopy (AES) is a dedicated surface analytical tool used to measure the presence and quantity of elemental species on the surface layer of solids. In this technique, the surface layer is on the order of angstroms thick.

AES was performed using a FISONS/VG Microlab 310D microscope. The pre-exposed sample was fractured under ultra-high vacuum with a bend impact stage. Half of the sample was transferred to the analysis chamber of the instrument and the fracture face examined using an electron beam at 10 kV. Analyses were performed in the multipoint mode, with each analysis point covering a few hundred square nm. Depth profiling was performed using a 3kV argon ion beam at a profiling rate of 3.4

μm/min. The profiles for Ni, S and O at points ahead and just behind the transgranular to intergranular transition.

As shown in Figure 27, a total of five points were analyzed. Two points, (Numbers 4 and 5), were profiled just ahead of the crack front, in the transgranular region and three points, (Numbers 1, 2, and 3), were profiled just behind the crack front in the intergranular region. Although these profile measurements were conducted without standards, and are thus not completely accurate, it is nonetheless shown that an enrichment of O and S occurred in the intergranular region near the crack front and not in the transgranular region ahead of the crack front. Indications of the heavy metals Sb and Pb were not observed. Unfortunately, however, the sensitivity for Sb in AES is low and the primary Sb peak may be eclipsed by the overlap with the Cr peak.

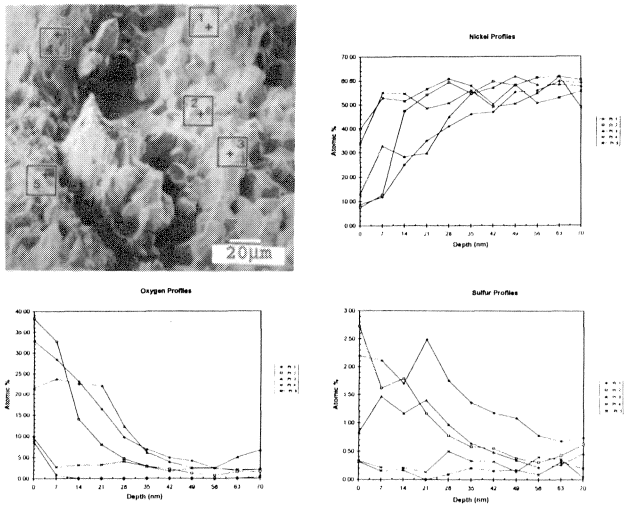


*Figure 27. Points Analyzed by Auger Electron Microscopy, in the Vicinity of the Crack Front of a Modified Waspaloy Stress-Rupture Bar. Exposure Condition: T = 1112°F, $T_{exp}$ = 3.5 hrs.*

Elements such as S, Sb, and Pb are of concern due to their potential deleterious effect on the mechanical properties of Ni-base alloys. For instance, sulfur has been shown to embrittle nickel alloys [12]. Steam turbine casing bolts made of Nimonic 80A have been found to exhibit intercrystalline stress corrosion cracking resulting from sulfide containing lubricants and steam impurities [13].

In alloy steels, Sb has been documented as an important contributor to temper embrittlement [14]. The enrichment of such alloy additions as Mn, Cr, and Mo during austenitizing is believed to lead to the enhanced segregation of embrittling elements as P, As, Sb, or Sn by chemical interaction. The result of this segregation is a changeover from cleavage to intergranular brittle fracture. Metalloids such as Sb and Pb have been shown to adversely affect the ductility of Ni and Ni-base superalloys [15, 16].

The inability to detect Sb and Pb on the intergranular fracture surfaces would at first suggest that only O and S were the important contributors. However, if sulfur was in fact a major contributor to the rapid fracture, it would be assumed that the specimens that were subjected to S-impregnation would have experienced a similar mode of failure. In fact though, this did not occur. Instead, the effect of S-impregnation appeared to only manifest itself in increasing the amount of creep that occurred.

The rapid fracture of the specimens tested under Set #3, infers that failure occurred as a result of embrittlement or stress corrosion cracking (SCC). As compared to steels and stainless steels, Ni-base alloys generally exhibit improved resistance to environmental embrittlement [17]. However, under combined specific environmental conditions and tensile stresses, Ni-base alloys can exhibit environmentally induced embrittlement. This embrittlement is thought to occur by either SCC or hydrogen embrittlement.

The following types of environments have been found to promote the SCC of Ni-base alloys [17]: high-temperature halogen ion solutions, high-temperature waters, high-temperature alkaline solutions, near ambient temperature polythionic acid solutions, and environments containing acids and hydrogen sulfide ($H_2S$).

One form of hydrogen embrittlement is manifested in brittle (usually intergranular) delayed fracture. Fully annealed Ni-base alloys are generally immune to this phenomenon. Hydrogen embrittlement is, however, important for Ni-base alloys for that the strength level has been increased by either cold working or heat treatment. In addition, only low iron containing alloys, greater than 10 percent Fe, are significantly affected.

The comments with respect to hydrogen embrittlement are particularly relevant with regards to the role elements such as Sb play as recombination poisons [18, 19]. In both aqueous and gaseous environments, such a poison may act to retard the combination of hydrogen atoms to form diatomic hydrogen molecules. In the vicinity of a grain boundary, instead of evolving from the metal surface in molecular form, uncombined hydrogen atoms increase in number. Thus, there is a higher probability of atomic hydrogen absorbing into the metal lattice and eventually giving rise to hydrogen embrittlement.

It is interesting to note the difference in the H and $H_2$ partial pressures in the case of the partial and fully combusted flue gas situations. The theoretical equilibrium H and $H_2$ partial pressures for typical partial and fully combusted flue gas conditions is listed in Table 1. Under equilibrium conditions, the H partial pressures for partial CO combustion is at least five orders of magnitude greater than that under complete CO combustion. This number could theoretically increase, if in fact, Sb retards the formation of molecular hydrogen.

The purpose to the above discussion was to identify *possible* mechanisms that may be responsible for the rapid failure of specimens tested under Set #3 conditions. Identification of the exact mechanism is outside the scope of the intended research project. The important point raised from these tests however, is that a catalyst environment can induce rapid failure of Waspaloy specimens. Since the catalyst residue is found packed between the blade root and disk, similar conditions may exist in an actual operating power recovery turbine whereby environmentally assisted fracture is possible.

When viewed in the context of Fracture Mechanics, it can also be inferred that in catalyst environments, the fracture toughness of Waspaloy, $K_{IC}$, is significantly reduced. The highest plane-strain stress intensity factor value at that subcritical crack growth does not occur in a material statically loaded in an aggressive environment is designated $K_{ISCC}$. As will be shown in the next section, a value of $K_{ISCC}$, can be extracted from the data generated from Set #3 test results. The relevance and importance of the derived value of $K_{ISCC}$ will furthermore be demonstrated in the fracture mechanics model that was derived to explain the failures of blades that had formed oxide wedges.

## FAILURE MODEL

Blades that have experienced failure in the root land, have been found to contain oxide wedges. The existence of an oxide wedge is expected to act as a stress concentrator. In fact, the oxide wedge itself can be taken as a flaw or crack within the blade substrate material. When viewed in the context of fracture

mechanics, a stress-intensity factor can be calculated at the oxide wedge front. The magnitude of the stress-intensity is a function of both the oxide wedge shape and depth, as well as the applied stress acting perpendicular to the oxide wedge propagation direction.

In addition, to oxide wedge formation, the accumulation of catalyst residue within the gap between the blade root and disk is also expected to play an important role. As described in the previous section, Waspaloy, in the presence of catalyst debris, experiences rapid brittle fracture. From a fracture mechanics viewpoint, this can be looked upon as a reduction in the fracture toughness of Waspaloy.

A model, based on fracture mechanics, is proposed that incorporates both the effects of oxide wedge formation and the apparent reduction in fracture toughness of Waspaloy in contact with catalyst residue.

*Stress Intensity*

Due to the fact that a uniform stress field does not exist in the root land under consideration, (in the vicinity of the oxide wedge), an assessment of the stress intensity, ahead of an oxide wedge, was performed utilizing the method of weight functions. The weight function method has proven to be a useful and versatile method to calculating stress intensity factors. This is especially true for cracks subjected to nonuniform stress fields; including cracks in weldments or cracks under thermal loading, [20, 21, 22].

A stress intensity factor can be calculated by integrating the weight function m(x, a) and the stress distribution $\sigma(x)$ acting in the prospective crack plane. This results in the following expression for the stress intensity factor ($K_I$).

$$K_I = \int_o^a \sigma(x) m(x,a) dx \qquad (1)$$

The determination of the weight function m(x, a) requires a complex elastic analysis of the cracked body. As found in the literature, a number of weight function solutions exist for cracks in different geometric bodies and configurations; (e.g., surface elliptic cracks in a finite body, edge cracks in a semi-infinite plate, etc.) [20, 21, 22].

In the following discussion, the weight function utilized in calculating the stress intensity, at the oxide wedge tip, were obtained from Glinka [21], for an edge crack in a semi-infinite plate. The use of the weight function for such a geometry is deemed appropriate due to conservatively higher values of stress intensities obtained.

The weight function utilized was,

$$m(x,a) = \frac{2}{\sqrt{[2\pi(a-x)]}}\left[1 + 0.5693\left(1 - \frac{x}{a}\right) + 0.279375\left(1 - \left(\frac{x}{a}\right)^2\right)\right] \qquad (2)$$

In this equation, "a" is the oxide wedge depth, and "x" is the coordinate dimension, in the x direction, which contains the oxide wedge.

The stress field $\sigma(x)$ has to be determined for an uncracked body using an analytical, numerical or experimental method of stress analysis. In the case of an expander blade, the stress distribution, in the vicinity of an oxide wedge, was obtained through a finite element analysis. The shape of stress profile, in the plane containing the oxide wedge, is shown in Figure 28. From this stress profile, an analytic equation representing stress as a function of distance into the blade root, x, can be obtained,

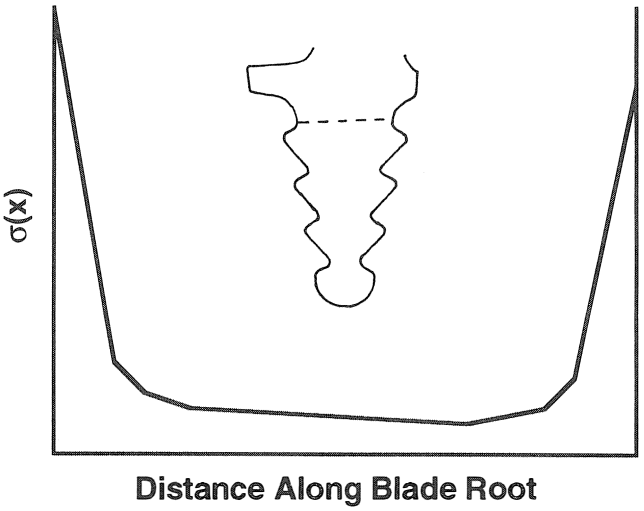


*Figure 28. Schematic Representation of the "Typical" Linearized Stress Profile Through the Blade Root Land in the Plane of an Oxide Wedge.*

$\sigma(x)$. Integrating the product of the stress distribution $\sigma(x)$ with the appropriate weight function, Equation (2), results in the stress intensity at the tip of the oxide wedge. The results of such an integration can be represented in a plot of stress intensity, $K_I$, *vs* oxide wedge depth, a (Figure 29).

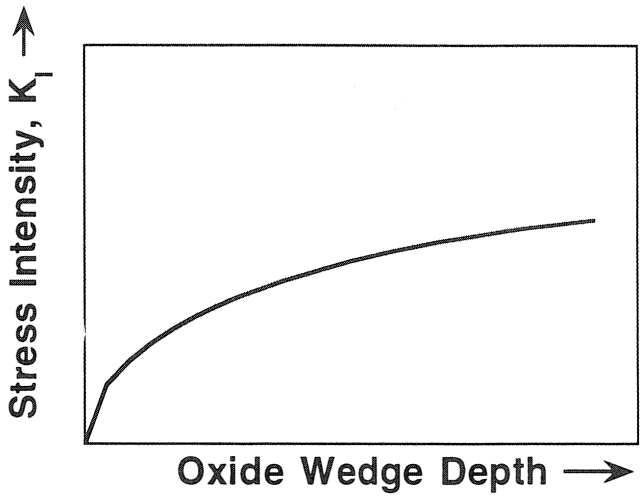


*Figure 29. Stress Intensity Profile, as a Function of Oxide Wedge Depth Penetration into the Blade Root Substrate.*

*Fracture Toughness*

As discussed earlier, testing of the modified stress-rupture bars, in contact with spent FCC catalyst, resulted in rapid brittle intergranular specimen failures. Failure times were typically on the order of minutes. Assuming that specimens exposed under the modified stress-rupture test phase exhibited brittle fracture, use was made of the analytical relationships that have been developed for a notched specimen in the determination of a stress intensity factor. Although a rigorous determination of a material's fracture toughness was not possible, it is felt that a bounding value of a materials fracture toughness, $K_{IC}$, may nonetheless be obtained. In that these values were obtained

under aggressive environments, the fracture toughness may more appropriately be described as $K_{ISCC}$.

It can be shown [23] which stress intensity, $K_I$, for a notched circular bar can be calculated. The stress intensity, $K_I$, is a function of the applied stress and both the notch and bar diameters. Based on this analysis, the stress intensities, for notched bars tested with catalyst can be calculated. Under the various stress loadings tested, there appeared to be a maximum stress intensity, above that the modified notch combination bars failed in a rapid brittle mode. For the purposes of this discussion, the critical stress intensity will be referred to as $K_{ISCC}$. The value of $K_{ISCC}$ tested in the presence of catalyst is significantly less than the value of $K_{IC}$, $\approx$ 100 Ksi(in)$^{1/2}$, measured for unexposed Waspaloy at elevated temperatures. It is important to recognize that the value of $K_{ISCC}$, can be treated as a material property. That is the fracture toughness determined for Waspaloy under catalyst corrosion tests can be applied to other geometries and loading conditions. When the value of $K_{ISCC}$ is superimposed on the plot for stress intensity *vs* oxide wedge depth, Figure 30, it has been found that for blades that have failed, the applied stress intensity either equals or exceeds $K_{ISCC}$. Conversely, for blades that *did not* fail, and yet contained oxide wedges, the stress intensities of the oxide wedge were found to be *less* than $K_{ISCC}$.

The results of such an analysis, obtained from three separate units is shown in Figures 30, 31, and 32. In Figure 30, two blades from the same unit, were compared; one intact and one failed blade. The results shown in Figures 30 through 32 confirm the validity of the model.

The above analysis does not infer that rapid, instantaneous, failure occurs when the $K_I$ at the oxide wedge tip exceeds $K_{ISCC}$. It is instead envisioned that under actual conditions, a likely failure scenario involves the local environment adversely reducing Waspaloy's fracture toughness in the region ahead of the oxide wedge. Once the toughness has been reduced below $K_{ISCC}$, an intergranular crack initiates and grows. The crack will then grow until it encounters material within the blade root that has a higher fracture toughness, at that point crack growth is arrested. Given time, the local environment will again lower the fracture toughness ahead of the crack. When the fracture toughness is less than $K_{ISCC}$, crack growth will resume.

This process is expected to be repeated until total blade failure occurs. It is also important to recognize, which as the crack increases in size, the stress intensity ahead of the crack also increases. Thus the crack, in effect, can grow into "tougher" material.

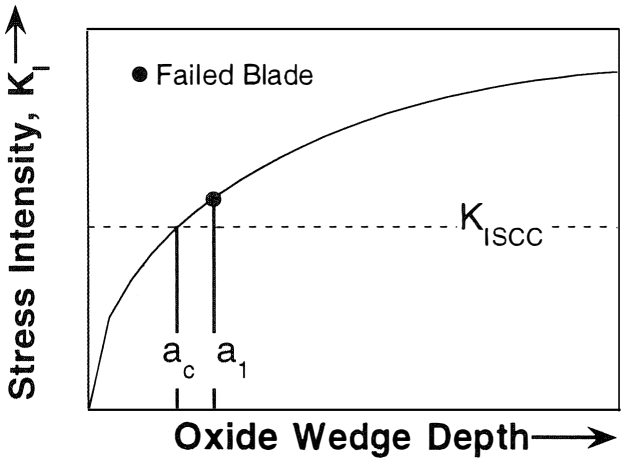


*Figure 31. Stress intensity profile* vs *oxide wedge depth for Unit B. In the failed blade $a_1$ was found to exceed $a_c$.*

## PROTECTIVE MEASURES

As a result of the blade failures described, three approaches were taken to resolve the problem. One approach was to determine the details of the failure mechanism. The results of this effort have been described. In the second approach, a means to create a positive steam barrier to flue gas and catalyst ingress was developed. The third approach was to investigate the feasibility of applying a protective diffused chromized coating to the blade root. The results of efforts to develop the protective steam barrier and chromized coating will be addressed.

### *Steam Barrier System*

The preventive measure that is presently being used by the authors company is the steam barrier system. This system has been successfully incorporated into a unit that has been in operation for well over one year. The principle behind the steam barrier design is to inject steam into the inlet and exhaust

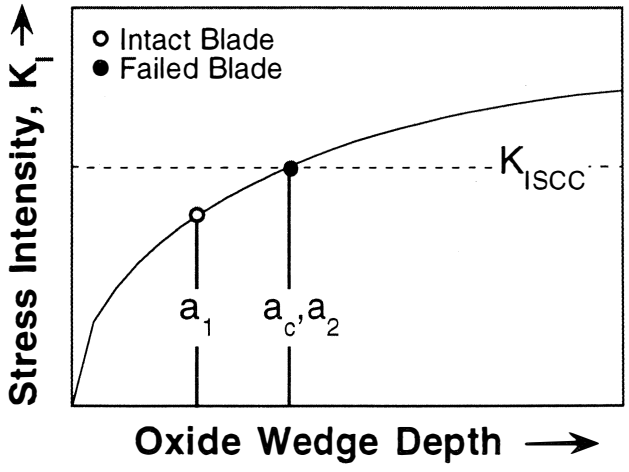


*Figure 30. Stress Intensity Profile* Vs *Oxide Wedge Depth for Unit a. Critical oxide wedge depth for failure was defined as $a_c$. In the failed blade $a_2$ was found to exceed $a_c$. In an intact blade, $a_1$, was less than $a_c$.*

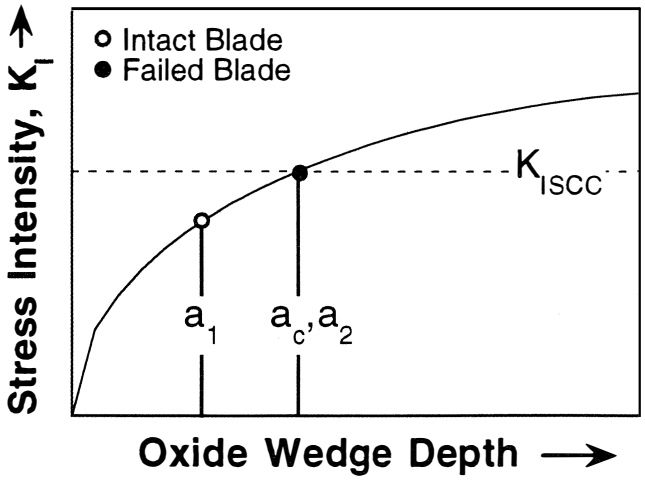


*Figure 32. Stress Intensity Profile* vs. *Oxide Wedge Depth for Unit C. Observed Wedge Depth, $a_1$, From an* Intact *Blade Found $a_1$ to be Less Than $a_c$.*

chambers to prevent the ingress of gas and catalyst into the disk/blade root area. In such an approach, the potential for high temperature corrosion can be eliminated or greatly reduced. The theory and sealing flow requirements for a shrouded, rotating disk with external swirling flow has been described [23].

The factors that affect the ingress of flue gas into the blade root area, and the quantity of steam required to ensure a positive barrier include the axial gap at the rim of the disk, the radius of the disk rim, and the rotating speed of the expander. In addition, the sealing fluid properties (i.e., steam) and the swirling external flow also affect flue gas ingress and the quantity of barrier fluid required. To achieve a complete barrier, separate piping and nozzle systems must be incorporated into the power recovery in order to ensure that flue gas ingress does not occur on both the upstream and downstream sides of the rotor disk. Based on model test data and theoretical calculations, the sealing flow requirements can be calculated to prevent flue gas ingress.

*Diffused Chromium Enrichment*

Another prevention method that is being considered is the application of a coating to the blade/disk root area to prevent/or greatly reduce the potential for high temperature corrosion. The application of coatings has enabled the use and life extension of components exposed to harsh, corrosive environments. Chromium and aluminum rich coatings are used to improve the oxidation resistance of iron and nickel base superalloys. Although coatings offer a means of achieving or improving the corrosion resistance behavior of a material, drawbacks can exist. For instance, the creation of a new surface or interface, can lead to other problems, such as fatigue crack initiation sites.

The mechanical properties of the coating can also have undesirable characteristics. For example, the application of an aluminide coating to a Ni-base superalloy results in the formation of an oxidation resistant β NiAl layer. Depending on the nickel composition, β aluminides undergo a ductile to brittle transition (DBTT) at temperatures from 1400 to 1800°F [24]. At low temperatures, due to its brittle nature, small strains are expected to crack the coating. Cracks in the coating are in turn expected to propagate into the superalloy. Aluminide coatings also do not provide sufficient protection in sulfidizing or hot corrosive environments [25].

Due to the improved resistance to sulfidizing attack and inherent ductility, the application of a chromium rich coating was investigated. An additional objective was to achieve an increase in the surface activity of chromium, in the alloy, without the formation of an interface between the coating and the metallic substrate. By raising the surface activity of chromium, this results in effectively shifting the kinetic boundary (KB), as shown in Figure 18, to the left, and thus promoting the formation of a protective $Cr_2O_3$ layer. The formation however, of an outer α-chromium layer is undesirable, in that such a layer is brittle and prone to cracking. It is important that this layer be removed after the chromizing treatment.

To achieve the desired objective, the pack cementation process was selected. A test matrix, based on pack composition, temperature and time was conducted. The most promising coating or Cr-enrichment was selected for further corrosion and mechanical test evaluation. Figure 33 illustrates the increased chromium content of a chromized Waspaloy sample. Corrosion testing has shown that the chromized layer or enrichment, is in fact significantly more resistant to sulfidizing attack than Waspaloy.

In one series of high temperature corrosion tests, where both chromized and nonchromized Waspaloy samples were tested under highly sulfidizing conditions, the chromized Waspaloy samples were found to exhibit a 100 fold decrease in the amount

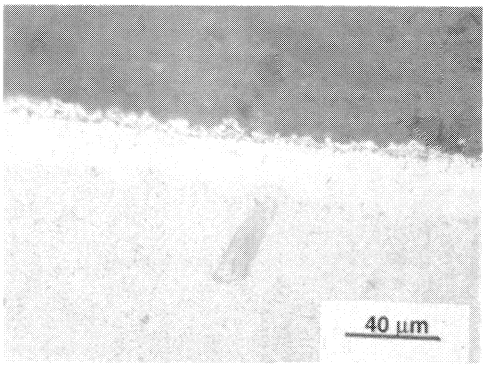


| Distance from Surface, Microns | Weight % Al | Ti | Cr | Fe | Ni | Co | Mo |
|---|---|---|---|---|---|---|---|
| 2 | 0.3 | 0.2 | 84.8 | 3.0 | 6.1 | 1.6 | 3.9 |
| 5 | 1.4 | 1.0 | 33.7 | 7.4 | REM | 10.9 | 2.9 |
| 8 | 0.3 | 0.3 | 32.7 | 7.2 | REM | 11.2 | 3.0 |
| 11 | 0.7 | 5.5 | 29.3 | 6.4 | REM | 10.4 | 2.9 |
| 14 | 0.7 | 0.8 | 28.1 | 5.6 | REM | 11.8 | 2.9 |
| 17 | 0.9 | 1.3 | 26.8 | 5.3 | REM | 11.3 | 3.0 |
| 20 | 0.8 | 1.3 | 25.8 | 4.2 | REM | 12.1 | 3.2 |
| 23 | 1.2 | 1.7 | 24.6 | 3.6 | REM | 11.9 | 3.6 |
| 26 | 1.3 | 2.1 | 23.2 | 3.2 | REM | 12.2 | 3.3 |
| 29 | 1.3 | 2.3 | 21.7 | 2.8 | REM | 12.4 | 3.3 |
| 32 | 1.5 | 2.7 | 21.3 | 2.7 | REM | 12.6 | 3.2 |
| 35 | 1.4 | 1.9 | 22.1 | 1.9 | REM | 14.3 | 3.9 |

*Figure 33. Illustration of Chromized Layer on Waspaloy.*

of corrosive attack, (as indicated by weight gain measurements). Metallographic examination found a protective $Cr_2O_3$ scale had in fact developed. By increasing the corrosion resistance, the formation and subsequent thickness of a stratified corrosion product layer, which in turn results in oxide wedge formation, is expected to be reduced as compared to nonchromized Waspaloy. Numerous tests were done at the senior author's company over the past three years to develop the optimum diffused coating and operational parameters to achieve the desired surface chemistry. This aspect of the development was critical since the objective is to diffuse chromium into the alloy without the formation of any detrimental phases. These phases can adversely affect the high temperature corrosion resistance of the coated Waspaloy and, in certain cases, drastically affect the mechanical integrity of the rotating Waspaloy components. The coating development is in its final stages of testing and should be released this year.

## CONCLUSIONS

The corrosion product morphologies that have been observed to develop in the roots of blades used in power recovery turbines has been described. A significant difference was noted between units operating under partial and complete combustion modes. For instance, in units operating on partially combusted flue gases, the growth of "oxide wedges" has been found to create areas of stress concentration. The factors that are expected to contribute to corrosive attack are discussed. These factors include flue gas composition, catalyst accumulation in the gap between the blade root/disk and fretting. The presence of catalyst has been shown to significantly degrade the fracture toughness of Waspaloy.

A fracture mechanics based model was developed to rationalize the observed blade failures. This model incorporates the influence of oxide wedges, Waspaloy's reduced fracture toughness and the stress profile through the blade land. Preventative measures to alleviate or minimize the formation of a corrosion product, and in turn reduce the chances of failure, are described.

These measures include the use of a steam barrier system and chromized coatings.

## REFERENCES


1. Proceeding of the Elliott Co. International Power Recovery Seminar, Elliott Co., Jeannette, Pennsylvania (1979).
2. Nieskens, M., Khouw, F., Borley, M.., and Roebschlaeger, K-H. W., "Shell's Resid FCC Technology Reflects Evolutionary Development," Oil & Gas Journal, 37, pp. 37-44 (June 1990).
3. Sehitoglu, H. "Thermo-Mechanical Fatigue Life Prediction Methods," Advances in Fatigue Lifetime Predictive Techniques, ASTM STP 1122, Mitchell, M. R. and Landgraf, R. W., Eds., American Society for Testing and Materials, Philadelphia, pp. 47-76 (1992).
4. Birks, N., and Meier, G. H., *Introduction to High Temperature Oxidation of Metals*, London: Edward Arnold Publishers (1983).
5. Xu, H., Hocking, M. G., and Sidky, P. S., "Sulfidation-Oxidation Behavior of Alloy 800H in $SO_2$-$O_2$ and $H_2$-$H_2S$-CO-$CO_2$ Atmospheres," Oxidation of Metals, *41*, (1/2), pp. 81-101 (1994).
6. Xu, H., Hocking, M. G., and Sidky, P. S., "Sulphidation-Oxidation Behavior of a Ni-Co-Cr-Si Alloy in an $SO_2$ + $O_2$ Atmosphere," Oxidation of Metals, *39*, (5/6), pp. 371-388 (1993).
7. Tiearney, Jr., T. C., and Natesan, K., "Sulfidation-Oxidation of Advanced Metallic Materials in Simulated Low-Btu Coal-Gasifier Environments," Oxidation of Metals, *17*, (1/2), pp. 1-26 (1982).
8. Birks, N., and Meier, G. H., Private Communication.
9. Giggins, C. S., and Pettit, F. S., "Corrosion of Metals and Alloys in Mixed Gas Environments at Elevated Temperatures," Oxidation of Metals, *14*, (5), pp. 363-413 (1980).
10. Kofstad, P., *High Temperature Corrosion*, New York: Elsevier Applied Science, pp. 465-510 (1988).
11. Gilson, F., and McKay, D., "Passivate Metals in FCCU Feedstocks," Fuel Reformulation, pp. 51-54 (November/December 1993).
12. Johnson, W. C., Doherty, J. E., Kear, B. H., and Giamei, A.F., "Confirmation of Sulfur Embrittlement in Nickel Alloys," Scripta Metallurgica, *8*, pp. 971-974 (1974).
13. "New Materials for Advanced Steam Turbines, Volume 4: Testing of Superalloy Bolt Materials for Advanced Power Plants," EPRI Report TR-100979, *4*; Research Project 1403-15 (September 1992).
14. Capus, J. M., "The Mechanism of Temper Brittleness," Temper Embrittlement in Steel, ASTM STP 407, American Society for Testing and Materials, pp. 3-19 (1968).
15. White, C. L., and Padgett, R. A., "Effects of Sb, Sn, As, and P Additions on the High-Temperature Ductility of Ni," Scripta METALLURGICA, *16*, pp. 461-466 (1982).
16. Kent, W. B., "Trace-Element Effects in Vacuum-Melted Superalloys," Journal of Vacuum Science and Technology," *11*, (6), pp. 1038-1046 (Nov/Dec 1974).
17. Kolts, J. "Environmental Embrittlement of Nickel-Base Alloys," Metals Handbook 9th Edition, ASM International (Metals Park OH), pp. 647-652 (1987).
18. Latanision, R. M., "Physical Metallurgy of Nickel-Base Alloys as It Relates to Corrosion," Journal of Materials Engineering, *10*, (2), pp. 143-162 (1988).
19. Latanision, R. M., and Opperhauser, Jr., H., "The Intergranular Embrittlement of Nickel by Hydrogen: The Effect of Grain Boundary Segregation," Metallurgical Transactions, *5*, pp. 483-492 (February 1974).
20. Xu, W., and Carlsson, A. J., *Weight Functions and Stress Intensity Factor Solutions*, New York: Pergammon Press (1991).
21. Glinka, G., and Shen, G., "Universal Features of Weight Functions for Cracks in Mode I," Engineering Fracture Mechanics, *40*, (6), pp. 1135-1146 (1991).
22. Shen, G., and Glinka, G., "Weight Functions for a Surface Semi-Elliptical Crack in a Finite Thickness Plate," Theoretical and Applied Fracture Mechanics, *15*, pp. 247-255 (1991).
23. Izenson, M.G., Swift, W. L., and Aungier, R. H., "Sealing Flow Requirements for a Rotating Disk with External Swirling Flow," Presentation at the International Gas Turbine and Aeroengine Congress and Exposition, The Hague, Netherlands, pp. 1-12 (June 1994).
24. Grisaffe, S. J., *Coatings and Protection, The Superalloys*, Sims, C. T., and Hagel W. C., Editors, New York: John Wiley & Sons, pp. 341-370 (1972).
25. Godlewska, E., and Godlewska, K., "Chromaluminizing of Nickel and Its Alloys," Oxidation of Metals, *22*, (3/4), pp. 117-131 (1984).